THESIS FOR THE DEGREE OF DOCTOR OF PHILOSOPHY IN SOLID AND
STRUCTURAL MECHANICS

Numerical methods for multiscale modelling of fibre composites

ELIAS BÖRJESSON

Department of Industrial and Materials Science
CHALMERS UNIVERSITY OF TECHNOLOGY

Göteborg, Sweden 2024

Cover:
A beam at the macroscale with two delaminating interfaces. The colours of the elements represent their current (adaptive) configuration. The mesoscale is represented by a 2D woven textile composite, with parts of the matrix discretisation visualised (blue). The arrows represent exchange of information between the macroscale and mesoscale (prolongation and homogenisation).

Numerical methods for multiscale modelling of fibre composites
ELIAS BÖRJESSON
Department of Industrial and Materials Science
Chalmers University of Technology

ABSTRACT

Fibre composite materials are inherently heterogeneous, often characterised by a complex internal substructure that includes various material phases and interfaces. The intricate substructure, at both the microscale and mesoscale, gives rise to a wide range of damage mechanisms that grow and propagate before they eventually manifest at the macroscale. To accurately capture and predict fibre composite behaviour at the macroscale, a comprehensive multiscale approach which includes information from the subscale is essential. This thesis addresses key challenges for multiscale modelling of fibre composites, focusing on the development of numerical methods at the macroscale, mesoscale, and the coupling between them.

In order to incorporate information from the mesoscale into the model at the macroscale, we develop a two-scale computational homogenisation framework. As fibre composites are often used in thin-ply applications, the homogenisation framework is developed for plate elements, specifically plates with Reissner–Mindlin kinematics. Moreover, a vital part for any effective homogenisation framework is to establish accurate prolongation and homogenisation constraints. To this end, we demonstrate how Variationally Consistent Homogenisation (VCH) can be employed to derive constraints which link the mesoscale and macroscale in a kinematically consistent manner.

At the macroscale, we address the challenges related to efficient and robust modelling of delamination in multilayered composites. Current state-of-the-art modelling techniques typically resolve each individual layer using multiple solid elements in conjunction with cohesive zone elements at the laminae interfaces, which results in computationally demanding models. In response to this, we develop an isogeometric shell element which can adaptively refine its through-thickness discretisation in areas where delamination is active. Thereby, the computational effort is kept low. To address the convergence issues typically encountered when simulating brittle delamination, we develop an arc-length solver that is augmented with the dissipation rate of the system. In this manner, we are able to trace the initiation and propagation of multiple delamination in a robust manner.

For accurate mesoscale modelling, it is crucial to include a detailed representation of the geometry and material constituents (fibre and matrix phases). However, incorporating high levels of geometric detail of the mesoscale structure presents significant challenges for meshing software, as it complicates the generation of good quality meshes. To address these challenges, we investigate the use of Immersed Boundary Methods, whose primary advantage is the automation of the discretisation process. We propose a modelling framework that streamlines the discretisation process for mesoscale models, demonstrating its ability to homogenise stiffness properties and accurately predict the subscale stress field.

Keywords: Multiscale Modelling, Fibre Composites, Isogeometric Analysis, Immersed Boundary Methods, Finite Cell Method, Mesoscale modelling, Path-following solver

Preface

Acknowledgements

THESIS

This thesis consists of an extended summary and the following appended papers:

Paper A   E. Börjesson, F. Larsson, K. Runesson, J. J. C. Remmers, and M. Fagerström. Variationally consistent homogenisation of plates. *Computer Methods in Applied Mechanics and Engineering* **413** (2023), 116094

Paper B   E. Börjesson, J. J. C. Remmers, and M. Fagerström. An adaptive isogeometric shell element for the prediction of initiation and growth of multiple delaminations in curved composite structures. *Computers & Structures* **260** (2022), 106701

Paper C   E. Börjesson, J. J. C. Remmers, and M. Fagerström. A generalised path-following solver for robust analysis of material failure. *Computational Mechanics* **70** (2022), 437–450

Paper D   E. Börjesson, C. V. Verhoosel, J. J. C. Remmers, and M. Fagerström. Meso-scale modelling of complex fibre composite geometries using an immersed boundary method. *Finite Elements in Analysis and Design* **242** (2024), 104262

The appended papers were prepared in collaboration with the co-authors. The author of this thesis played a leading role in the work, contributing significantly to the formulation of the theory, developing the numerical implementations, conducting the numerical simulations, and drafting the manuscripts.

CONTENTS

Part I
Extended summery

1 Introduction

The ability to design lightweight structures is crucial in many industries, including aerospace, automotive, and sports technology [1, 2]. A class of material that possesses favourable lightweight characteristics is fibre reinforced composites. These materials consist of strong and light fibres (e.g., carbon, glass, kevlar) embedded in a binding polymer matrix (e.g., epoxy). Fibre composites offer numerous advantages, for instance, they exhibit excellent stiffness-to-weight and strength-to-weight ratios, and can be tailored to obtain desired material properties for specific applications.

Despite their advantages, fibre composites present significant challenges in modelling and simulation [3]. These challenges manifest as difficulties in, for example, accurately predicting the various failure mechanisms (damage initiation and propagation), in conjunction with computationally efficiency. These challenges (among others) hinder the broader adoption of fibre composites in various products, as material and structural analysis through Computer Aided Engineering (CAE) are crucial for the product development process in many industries. Consequently, there is a need for (continued) research into efficient and accurate numerical simulation tools to support engineers in developing components in fibre composite materials.

One contributing factor to the significant challenges in modelling fibre composite structures is the heterogeneous and complex nature of the substructure at the meso- and microscale. Depending on the specific *fibre architecture* (i.e. the fibre and matrix configuration at the subscale), a wide range of damage phenomena can occur, such as matrix cracking, fibre kinking, and delamination. The heterogeneity and complexity of the subscale highlights that adopting a multiscale perspective, by explicitly incorporating details from the subscale structure into the macroscale model, would be beneficial for analysis and design. Accordingly, the overarching goal of this thesis is to investigate and provide new insights into modelling aspects at both the macroscale and subscale levels (here, we specifically focus on the mesoscale).

The following subsections provide a general overview of various modelling aspects and challenges encountered at macro- and mesoscale levels, and the coupling between them, which will be used to motivate the research scope of this thesis.

1.1 Multiscale modelling via computational homogenisation

Fibre composites exhibit a heterogeneous structure, spanning multiple hierarchical scales across the micro-, meso-, and macro-level. This heterogeneous and hierarchical nature introduces challenges in understanding and predicting composite behaviour; both in terms
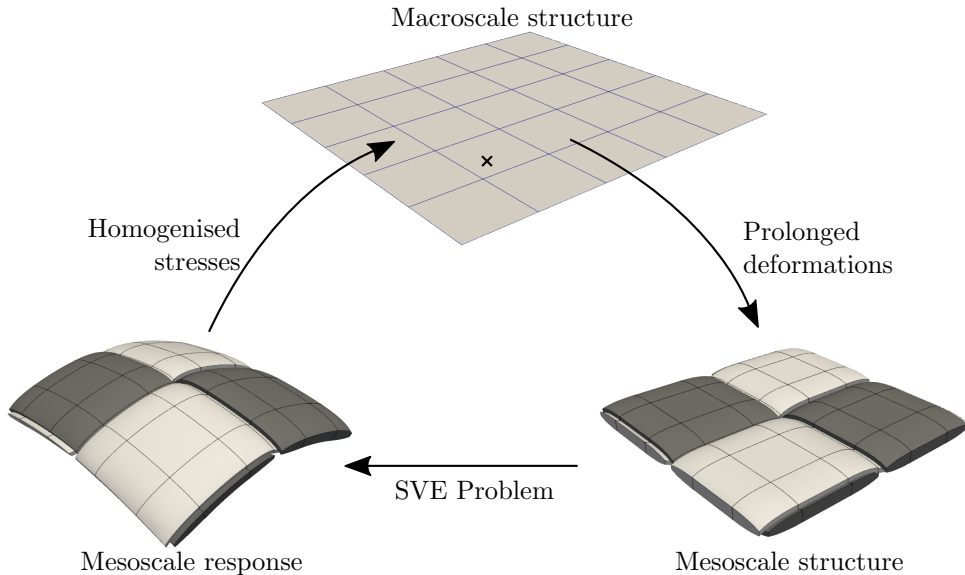
Figure 1.1: *Illustration of computational homogenisation.*

of anisotropic elastic behaviour and, more critically, in damage mechanisms such as matrix cracking, fibre kinking and breakage, or delamination. Consequently, it is important to develop multiscale modelling frameworks that include the behaviour at the mesoscale with the overall response at the macroscale.

A popular multiscale approach is Computational Homogenisation [4], wherein the constitutive behaviour at a material point on the macroscale is derived by solving a boundary value problem on a statistical or representative volume element (SVE or RVE) of the substructure. For a visual representation of computational homogenisation, see Figure 1.1. Two advantages of computational homogenisation include: the macroscopic local constitutive equations can be derived directly from the solution of the corresponding microscale boundary value problem, and one may include arbitrary subscale complexity, including physically non-linear and time-dependent characteristics. Research on computational homogenisation techniques has predominantly been focused towards methods where solid/continuum elements are used on the macroscale. However, fibre composite materials are frequently employed in thin shell applications, which are more appropriately modelled using plate or shell elements. In response to this, research efforts over the past two decades have begun to address computational homogenisation techniques specifically tailored to structural elements such beams, plates, and shells [5–7]. Nonetheless, further research is still required in this area and is addressed in this thesis.

1.2   Fibre composite modelling on the macroscale

Fibre composite modelling at the macro level involves trying to predict the structural properties and response (e.g. structural stiffness, risk of damage initiation, crashworthiness) of composite structures under various loading conditions. A common approach to model thin shell composite structures is to use equivalent single-layer (ESL) shell elements, where the composite material properties have been homogenised to the midsurface of a shell element. This modelling approach has generally demonstrated the ability to accurately and efficiently predict the overall stiffness and in-plane stresses of structural components, see e.g. [8]. Moreover, these models can be combined with failure criteria such as LARC [3], to predict when the material and structure fails. A shortcoming of ESL models, however, is that they do not resolve the through-thickness properties in a detailed manner, which limit their accuracy and applicability to model the different failure mechanisms experienced by fibre composites.

One failure mechanism that is prevalent in layered/laminated fibre composites is delamination. As indicated by the name, delamination occurs in layered structures (e.g., unidirectional (UD) layer composites), where cracks form and propagate between layers. Because delamination involves the separation of individual laminae, it is impossible to represent this with efficient shell models such as ESL. Therefore, the preferred way of modelling delamination is to use so-called Layer-Wise (LW) models, where each individual layer is represented by one or more solid elements, together with cohesive zone elements at each layer interface. For a visual representation of a LW model, see Figure 1.2a [9]. While LW models accurately capture the kinematics of the delamination phenomenon and have been used in many applications, the computational demand is significant, as UD fibre composites can consist of 10-100 layers.

Another challenge with modelling delamination in fibre composites is that it generally creates a brittle failure event. As with all brittle failures, it is typically difficult to obtain converged results in incremental quasi-static simulations beyond the maximum force peak [10]. Consequently, it is even more difficult to trace the full equilibrium path of the failure event. This limitation means that a significant amount of important information about the progressive failure event is lost.

1.3   Fibre composite modelling on the mesoscale

Mesoscale modelling focuses on the detailed representation of the internal structure of textile fibre composite materials, where the interactions between impregnated fibre bundles and the polymer matrix are explicitly considered, see Figure 1.2b which depicts the bundles in a woven composite. Note that in mesoscale models, the individual fibre filaments are not accounted for, but rather a homogenised representation of a collection of filaments (bundles) is used. These mesoscale models are used to obtain homogenised stiffness properties [11], monitor stresses and strains [12], or to investigate failure and damage mechanisms [13].

In order to be able to make accurate predictions with mesoscale composite models, it is essential to include a detailed representation of the geometry of the bundles and the

(a) *Layer wise model.* (b) *Mesoscale structure.*
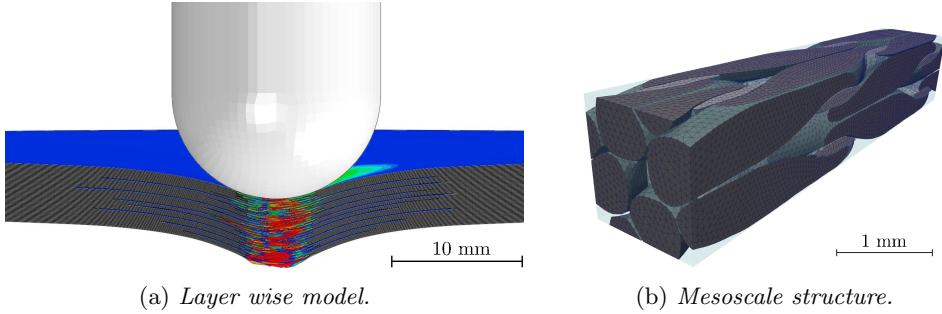
Figure 1.2: *Two fibre composite models at differnet scales. (a) A layer-wise model at the macroscale [9]. (b) A meshed mesoscale structure of a 3D-woven composite [21].*

matrix, as well as their interfaces [14]. Consequently, there is substantial research devoted to the generation of geometries for different fibre composite materials. For instance, TexGen and WiseTex are commonly used for generating planar and 3D weave composite geometries [15, 16], while other authors focuses on the generation of realistic 3D composite geometries through process simulation [17–19].

Irrespective of their fibre composite architecture and how it is generated, the mesoscale geometry can often be classified as "complex." Fibre bundles are typically closely situated, leading to small gaps and sharp angles between them. These geometric features pose significant challenges during the meshing process, particularly in pure matrix regions. This can result in an excessive number of elements, poor-quality elements, or situations where the mesh generator is unable to produce a mesh at all. Consequently, time-intensive manual intervention is often required to achieve desirable models. This is partially evidenced by the large number of authors who employ automatic voxel meshing procedures to circumvent the difficulties associated with generating boundary-conforming meshes, see e.g. [20] and references therein.

1.4 Research scope

The purpose of this thesis is to investigate and bring new insights into numerical modelling methods at both the macroscale and mesoscale levels, as well as the coupling between them. Based on the limitations and challenges described in the previous subsections, four research goals have been identified.

The first goal relates to the need for two-scale modelling framework for (thin) structural elements, in order to link the mesoscale mechanical response to macroscale models. As such, the first research goal is to:

- Develop a multiscale framework for plate-based computational homogenisation, and devise consistent prolongation and homogenisation conditions linking the macro- and subscale. This is addressed in **Paper A**.

Next, the delamination process of layered fibre-reinforced composites presents significant challenges for efficient evaluation, primarily due to the necessity of high-fidelity

models. Moreover, quasi-static simulations of brittle delamination (and other failure mechanisms), using incremental- and Newton-based solvers, often fail to convergence past the force-peak when structural failure initiates. Consequently, the second and third research goals, pertaining the macroscale, are to:

- Develop an isogeometric shell model that can adaptively refine its discretisation at arbitrary interfaces through the thickness, with the aim of creating an efficient shell model with refined areas only where the delamination initiates and propagates. This is addressed in **Paper B**.

- Develop a dissipation based path-following solver which can trace the full failure event and improve convergence in quasi-static simulations of delamination and brittle material failures. This is addressed in **Paper C**.

Finally, as the geometric features of mesoscale models bring considerable challenges in the discretisation/meshing process, there is a need of modelling approaches which can simplify the discretisation process of these structures. The forth research goal, pertaining to the mesoscale, is therefore to :

- Develop and investigate the use of immersed boundary methods for the modelling of complex mesoscale structures of textile fibre composites. The goal is to obtain a method that automates the meshing procedure of complex subscale geometries. This is addressed in **Paper D**.

1.5   Limitations

The development of the plate-based computational homogenisation framework in **Paper A**, the macroscopic shell **Paper B**, and the mesoscale modelling approach in **Paper D**, can in the current form be seen as stand-alone pieces of a puzzle. The individual papers propose solutions to address key challenges within each domain, but are currently not connected to demonstrate their feasibility in a coupled multiscale approach.

Furthermore, the following key limitations have been identified for each research goal and related paper.

- In **Paper A**, we do not consider homogenisation of non-linear material behaviour, but focus on demonstrating convergence properties of homogenised plate stiffness properties for linear elastic materials. Furthermore, we only consider prolongation and homogenisation for flat plates, where arbitrary curved shells are left for future work.

- In **Paper B**, we do not consider intralaminar damage, but limit our-selves to interlaminar damage (i.e. delamination). This is motivated by the fact that delamination is inherently a global phenomenon (layers separating from each other), which needs to be captured with models with refined through-thickness kinematics. Intra-laminar damage on the other hand, can often can be viewed local phenomenon that can be modelled with (for example) smeared crack models.

- In **Paper D**, we emphasise the development of a framework that simplifies the discretises process, whereby initially only linear elastic material behaviour on the macroscale will be considered when verifying the method.

1.6   Thesis outline

The thesis is divided into three parts relating to homogenisation, macroscale modelling and the mesoscale modelling. In Chapter 2, we present a kinematically consistent homogenisation framework for plate elements. Next, in Chapter 3, we present the developments of an isogeometric shell elements with adaptive through-thickness capabilities, for efficient modelling of delamination. In the same chapter, we also present the dissipation based arc-length solver for modelling of brittle failure in quasi-static simulations. In Chapter 4, a modelling framework based on the Finite Cell Method is presented, for streamlining the discretisation process of complex fibre composite mesoscale structures. Finally, the main conclusions are presented in chapter 5, and suggestions on future work is outlined.

2 Multiscale modelling for structural elements

Multiscale methods are techniques designed to bridge different length scales in the analysis of materials or structures. These methods are particularly beneficial when phenomena at smaller scales (such as the microscale or mesoscale) significantly influence the behaviour at larger scales (such as the macroscale), and when empirical constitutive models are insufficient. One widely recognised multiscale method is Computational Homogenisation [4], where the constitutive behaviour at a material point on the macroscale is derived (homogenised) from a detailed model and boundary value problem of the substructure (e.g., a mesoscale segment of a fibre composite). This can either be performed concurrently for all material points and time steps, if the subscale SVE is non-linear, or performed once in offline stage, if the SVE is linear elastic.

Fibre composite materials are often used in thin-shell applications, which are suitably modelled with plate or shell elements. As such, computational homogenisation techniques tailored to structural elements such as beams, plates, and shells is required. The following subsection provides a short overview of multiscale frameworks specifically designed for structural elements.

2.1 Computational homogenisation for structural elements

The first publications on computational homogenisation techniques for structural elements is attributed to Geers et al. [22], who developed a multiscale framework for Reissner-Mindlin type shells. Shell-based homogenisation was later extended to other shell theories, e.g. Kirchhoff-Love shells in [7], and 7-parameter shell model in [23]. The aforementioned homogenisation frameworks were demonstrated to work well for various micro-structures. However, in a study conducted by Främby et al. [24], it was noted that when the length-to-height aspect ratio of the SVE became large, the homogenisation of transverse shear stresses breaks down. Specifically, the transverse shear stiffness becomes under predicted. The phenomenon is reasonably well understood; Klarmann et al. [5] showed that a prolongation of macroscopic transverse shear strains on the SVE lateral faces, creates an unbalanced linear moment distribution, which suppresses the transverse shear deformation at the sub scale.

The deficiencies in the homogenisation of transverse shear stiffness has been identified by other authors as well, see e.g. [5, 6, 25], and various solutions has been proposed therein. While achieving satisfactory results, the proposed methods often use a-priori assumptions on the macro- and subscale, or add a-posteriori constraints to compensate for erroneous shear responses. However, as we show in **Paper A**, it is possible to derive a kinematically consistent homogenisation framework for Reissner-Mindlin type plates, without any a-priori specification of knowledge of the macro- or subscale problems, using Variationally Consistent Homogenisation (VCH) [26]. VCH provides a framework to derive consistent prolongation and homogenisaiton conditions for multi-physics problem [27], or for non-standard kinematics [28] (as in the case for plates kinematics).

2.2 Variationally consistent homogenisation for plates

The derivations in VCH start from a single scale (fully resolved) problem, from which the macroscale and subscale problems can be consistently derived from. The fully resolved problem is in this case represented by the plate-like body in Figure 2.1a, with domain Ω, midsurface A and thickness h. The boundary of Ω is divided into an edge surface Γ, and a top surfaces γ. We consider Dirichlet boundaries on $\Gamma_D \in \Gamma$, and a prescribed traction $\boldsymbol{t}_{\mathrm{p}}$ on γ. The weak format of the elasticity problem for the fully resolved problem can be formulated as: find the displacements $\boldsymbol{u} \in \mathbb{U}$ such that:

$$\int_\Omega \boldsymbol{\sigma}(\boldsymbol{\varepsilon}[\boldsymbol{u}]) : \boldsymbol{\varepsilon}(\delta\boldsymbol{u}) \,\mathrm{d}\Omega = \int_\gamma \boldsymbol{t}_{\mathrm{p}} \cdot \delta\boldsymbol{u} \,\mathrm{d}\Gamma \quad \forall \delta\boldsymbol{u} \in \mathbb{U}^0, \tag{2.1}$$

where $\boldsymbol{\sigma}$ is the Cauchy stress, and $\boldsymbol{\varepsilon}(\boldsymbol{u}) = (\boldsymbol{u}\otimes\boldsymbol{\nabla})^{\mathrm{sym}}$ is the linear strain tensors. Moreover, $\mathbb{U}$ and $\mathbb{U}^0$ are sufficiently smooth spaces that fulfill the boundary conditions.

The goal of two-scale computational homogenisation frameworks is to solve for smooth fields on the macroscale, in this case the plate-based fields such as deflection or cross-sectional rotation, without explicitly resolving the substructure on the subscale. As a step towards acquiring a two-scale formulation, we introduce a split of the displacement $\boldsymbol{u}$, into a macroscopic part, $\boldsymbol{u}^{\mathrm{M}}$ and subscale (or fluctuation) part, $\boldsymbol{u}^{\mathrm{s}}$, according to $\boldsymbol{u} = \boldsymbol{u}^{\mathrm{M}} + \boldsymbol{u}^{\mathrm{s}}$. The same split is assumed for the test function $\delta\boldsymbol{u}$.

Next, to further deviate from a single scale formulation, we introduce the SVE domains $\Omega_\square$, see Figure 2.1b, for each macroscopic point in A, and introduce the running average approximation:

$$\int_\Omega f \,\mathrm{d}\Omega \approx \int_A \langle f \rangle_\square \,\mathrm{d}A, \quad \langle f \rangle_\square \overset{\mathrm{def}}{=} \frac{1}{A\square} \int_{\Omega_\square} f \,\mathrm{d}\Omega,$$

$$\int_\gamma g \,\mathrm{d}\Gamma \approx \int_A \langle g \rangle_\square^\gamma \,\mathrm{d}A, \quad \langle g \rangle_\square^\gamma \overset{\mathrm{def}}{=} \frac{1}{A\square} \int_{\gamma_\square} g \,\mathrm{d}\Gamma, \tag{2.2}$$

where $\gamma_\square$ is the top surface of the SVE. We can now go from the single scale problem, to a two-scale formulation, by introducing the decomposition $\boldsymbol{u}^{\mathrm{M}} + \boldsymbol{u}^{\mathrm{s}}$ and the running average approximation in to Equation (2.1):

$$\int_A \langle \boldsymbol{\sigma}(\boldsymbol{\varepsilon}[\boldsymbol{u}^{\mathrm{M}} + \boldsymbol{u}^{\mathrm{s}}]) : \boldsymbol{\varepsilon}[\delta\boldsymbol{u}^{\mathrm{M}}] \rangle_\square \,\mathrm{d}A = \int_A \langle \boldsymbol{t}_{\mathrm{p}} \cdot \delta\boldsymbol{u}^{\mathrm{M}} \rangle_\square^\gamma \,\mathrm{d}A \quad \forall \delta\boldsymbol{u}^{\mathrm{M}} \in \mathbb{U}^{\mathrm{M},0}, \tag{2.3}$$

$$\int_A \langle \boldsymbol{\sigma}(\boldsymbol{\varepsilon}[\boldsymbol{u}^{\mathrm{M}} + \boldsymbol{u}^{\mathrm{s}}]) : \boldsymbol{\varepsilon}[\delta\boldsymbol{u}^{\mathrm{s}}] \rangle_\square \,\mathrm{d}A = \int_A \langle \boldsymbol{t}_{\mathrm{p}} \cdot \delta\boldsymbol{u}^{\mathrm{s}} \rangle_\square^\gamma \,\mathrm{d}A \quad \forall \delta\boldsymbol{u}^{\mathrm{s}} \in \mathbb{U}^{\mathrm{s}}. \tag{2.4}$$

Here, Equation (2.3) constitutes the macroscale problem, while Equation (2.4) defines the subscale problem. Before introducing the macroscale and subscale formulations, we will need to define kinematically consistent prolongation and homogenisaiton operators, for linking the two scales. This is done in the following subsections.
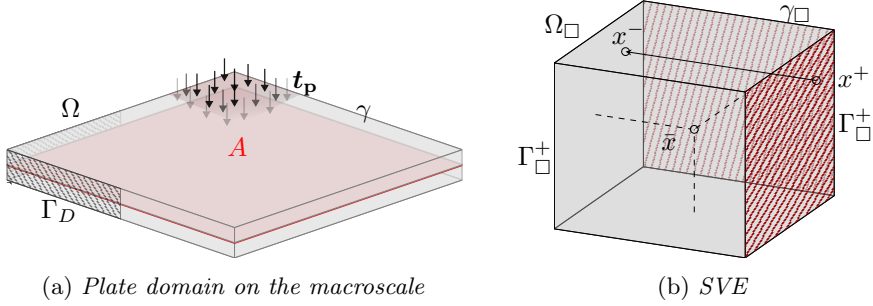
(a) *Plate domain on the macroscale*   (b) *SVE*

Figure 2.1: *The plate at the macroscale and the SVE at the subscale.*

Prolongation operator

The prolongation, $\boldsymbol{u}^M$ describes how the plate kinematical variables at a macroscale coordinate, $\boldsymbol{x} = x_1\boldsymbol{e}_1 + x_2\boldsymbol{e}_2 + z\boldsymbol{e}_3$, is projected on to the SVE. The prolongation operator is here obtained using first order homogenisation, meaning that we take the first order Taylor series expansion around the centroid of a SVE, $\bar{\boldsymbol{x}} = \bar{x}_1\boldsymbol{e}_1 + \bar{x}_2\boldsymbol{e}_2$. Employing Reissner-Mindlin kinematics, the following prolongation condition is established:

$$u_\alpha^M = \bar{u}_\alpha + \bar{h}_{\alpha\beta}[x_\beta - \bar{x}_\beta] - z\bar{\theta}_\alpha - z\bar{\kappa}_{\alpha\beta}[x_\beta - \bar{x}_\beta] \tag{2.5}$$

$$u_3^M = \bar{w} + \bar{g}_\alpha[x_\alpha - \bar{x}_\alpha], \tag{2.6}$$

where we have used index-notation with Greek letters signify the in-plate components 1 and 2. In Equation (2.6), $\bar{u}_\alpha$, $\bar{w}$, and $\bar{\theta}_\alpha$ are, respectively, the in-plane displacement, deflection, and cross-sectional rotation of the plate, evaluated at the coordinate $\bar{\boldsymbol{x}}$. Furthermore,

$$\bar{h}_{\alpha\beta} = \left.\frac{\partial \bar{u}_\alpha}{\partial x_\beta}\right|_{\boldsymbol{x}=\bar{\boldsymbol{x}}}, \quad \bar{\kappa}_{\alpha\beta} = \left.\frac{\partial \bar{\theta}_\alpha}{\partial x_\beta}\right|_{\boldsymbol{x}=\bar{\boldsymbol{x}}}, \quad \bar{g}_\alpha = \left.\frac{\partial \bar{w}}{\partial x_\beta}\right|_{\boldsymbol{x}=\bar{\boldsymbol{x}}}, \tag{2.7}$$

are the membrane strains, curvatures, and transverse shear strains, respectively. Note that these quantities only live on the midsurface of the reference body.

The fields $\bar{u}, \bar{\theta}, \bar{w}, \bar{h}, \bar{\kappa}, \bar{g}$ can be viewed has quantities that are known to the subscale boundary value problem. They represent different deformation modes prolonged on the SVE. As an illustration, in Figure 2.2, we evaluate Equation (2.6) on an unit square for in-plane stretch, bending and transverse shear, respectively.

Homogenisation operator

Next we consider the homogenisation of the macroscopic field variables and their gradients. For consistency, it is reasonable to require that the homogenisation of substructural deformations should recover the macroscopic field variables. As an example, consider the homogenisation of the in-plane deformation:

$$\bar{u}_{\square,\alpha}(\boldsymbol{u}) = \bar{u}_\alpha, \tag{2.8}$$

where $(\bullet)_\square$ denote homogenisation operators. Moreover, in order the have a unique decomposition of $\boldsymbol{u}^{\mathrm{M}}$ and $\boldsymbol{u}^{\mathrm{s}}$, it can be shown that the homogenisation operator must fulfil

$$\bar{u}_{\square,\alpha}(\boldsymbol{u}^{\mathrm{M}}) = \bar{u}_\alpha \tag{2.9}$$

$$\bar{u}_{\square,\alpha}(\boldsymbol{u}^{\mathrm{s}}) = 0. \tag{2.10}$$

Here, Equation (2.9) sets an explicit requirement on $\bar{u}_{\square,\alpha}$, whereas Equation (2.10) serves as a constraint for the subscale problem. Consequently, a natural selection of the homogenisation operators that satisfy Equation (2.9) is:

$$\bar{u}_{\square,\alpha}(\boldsymbol{u}) = \frac{1}{|\Omega_\square|} \int_{\Omega_\square} u_\alpha \, \mathrm{d}\Omega \tag{2.11}$$

$$\bar{w}_\square(\boldsymbol{u}) = \frac{1}{|\Omega_\square|} \int_{\Omega_\square} u_3 \, \mathrm{d}\Omega \tag{2.12}$$

$$\bar{\theta}_{\square,\alpha}(\boldsymbol{u}) = \frac{1}{|I_\square|} \int_{\Omega_\square} z u_\alpha \, \mathrm{d}\Omega \tag{2.13}$$

$$\bar{h}_{\square,\alpha\beta}(\boldsymbol{u}) = \frac{1}{|\Omega_\square|} \int_{\Gamma_\square^+} [\![u_\alpha]\!] n_\beta \, \mathrm{d}\Gamma \tag{2.14}$$

$$\bar{g}_{\square,\alpha}(\boldsymbol{u}) = \frac{1}{|\Omega_\square|} \int_{\Gamma_\square^+} [\![u_3]\!] n_\alpha \, \mathrm{d}\Gamma \tag{2.15}$$

$$\bar{\kappa}_{\square,\alpha\beta}(\boldsymbol{u}) = \frac{1}{|I_\square|} \int_{\Gamma_\square^+} z [\![u_\alpha]\!] n_\beta \, \mathrm{d}\Gamma \tag{2.16}$$

where $|\Omega_\square| = \int_\Omega \mathrm{d}\Omega$, $|I_\square| = \int_\Omega z^2 \, \mathrm{d}\Omega$ and $\boldsymbol{n} = n_\alpha \boldsymbol{e}_\alpha$ is the normal vector (from the surface $\Gamma_\square^+$). Furthermore, we have introduced the jump operator $[\![f]\!](\boldsymbol{x}^+) = f(\boldsymbol{x}^+) - f(\boldsymbol{x}^-)$,
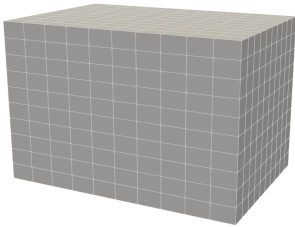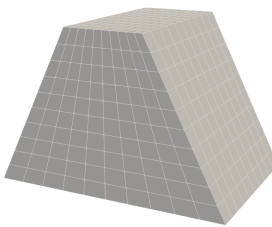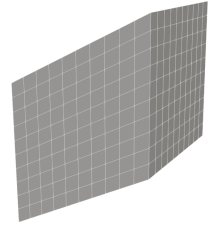
(a) $\bar{h}_1 = 0.5$ (b) $\bar{\kappa}_1 = 0.5$ (c) $\bar{g}_1 = 0.5$

Figure 2.2: *Visualisation of the prolongation $\boldsymbol{u}^M$ on a unit cube (SVE).*

where $\boldsymbol{x}^+$ is a point on the *image part* of the boundary $\Gamma_\square^+$, and $\boldsymbol{x}^-$ is the corresponding point on the adjacent face *mirror part* of the boundary $\Gamma_\square^-$ (c.f. Figure 2.1b). Finally, the icons next to the equations illustrates the different deformation modes that each homogenisaiton operator represents.

Macroscale problem

The weak form for the macroscopic plate problem can be established by introducing Equation (2.6) in to Equation (2.3). After some derivations, and using the simplifying assumption that $\boldsymbol{t}_p$ is uniformly distributed and only act in the out-of-plane direction, the macroscale problem can be formulated as: find $\bar{u}_\alpha \in \bar{\mathbb{U}}_u$, $\bar{w} \in \bar{\mathbb{U}}_w$ and $\bar{\theta}_\alpha \in \bar{\mathbb{U}}_\theta$ s.t.

$$\int_A \bar{N}_{\alpha\beta} \delta \bar{h}_{\alpha\beta} \, \mathrm{d}A = 0 \qquad \forall \bar{u}_\alpha \in \bar{\mathbb{U}}_u^0,$$

$$\int_A \bar{V}_\alpha \delta \bar{g}_\alpha \, \mathrm{d}A = \int_A \bar{q}^w \delta \bar{w} \, \mathrm{d}A \quad \forall \bar{w} \in \bar{\mathbb{U}}_w^0,$$

$$\int_A \bar{V}_\alpha \delta \bar{\theta}_\alpha + \bar{M}_{\alpha\beta} \delta \bar{\kappa}_{\alpha\beta} \, \mathrm{d}A = 0 \quad \forall \bar{\theta}_\alpha \in \bar{\mathbb{U}}_\theta^0,$$

where $\bar{\mathbb{U}}_\bullet$ and $\bar{\mathbb{U}}_\bullet^0$ are sufficiently smooth spaces that fulfil the boundary conditions, and $\bar{q}^w = \frac{1}{A_\square} \int_{\gamma_\square} t_{p,3} \, \mathrm{d}\Gamma$. Furthermore, $\bar{N}_{\alpha\beta}$ is the membrane forces, $\bar{M}_{\alpha\beta}$ are the bending moments, and $\bar{V}_\alpha$ are the transverse shear forces, defined as:

$$\bar{N}_{\alpha\beta} = \frac{1}{A_\square} \int_{\Omega_\square} \sigma_{\alpha\beta} \, \mathrm{d}\Omega, \quad \bar{M}_{\alpha\beta} = \frac{1}{A_\square} \int_{\Omega_\square} z\sigma_{\alpha\beta} + \sigma_{\alpha3}(x_\beta - \bar{x}_\beta) \, \mathrm{d}\Omega, \quad \bar{V}_\alpha = \frac{1}{A_\square} \int_{\Omega_\square} \sigma_{\alpha3} \, \mathrm{d}\Omega.$$
$$(2.17)$$

Interestingly, we can note that the moment $\bar{M}_{\alpha\beta}$ gets an extra contribution from the transverse shear stresses, with a lever that depends on the size of the SVE. Furthermore, from Equation (2.17), the two-scale coupling becomes apparent, as the plate forces are obtained from volume averages of the stresses from the subscale (SVE).

Subscale problem

The boundary value problem for the subscale can be established by performing a local approximation of each SVE domain $\Omega_\square$ in Equation (2.4), i.e. we consider each SVE as independent of each other. The subscale problem reads: find the displacement field $\boldsymbol{u}^s \in \mathbb{U}_\square^s$ s.t.

$$\frac{1}{A_\square} \int_{\Omega_\square} \boldsymbol{\sigma}(\boldsymbol{\varepsilon}[\boldsymbol{u}]) : \boldsymbol{\varepsilon}(\delta\boldsymbol{u}^s) \, \mathrm{d}\Omega = \frac{1}{A_\square} \int_{\gamma_\square} \boldsymbol{t}_p \cdot \delta\boldsymbol{u}^s \, \mathrm{d}\Gamma, \quad \forall \delta\boldsymbol{u}^s \in \mathbb{U}_\square^s$$

subjected to

$$\bar{u}_{\square,\alpha}(\boldsymbol{u}^s) = 0, \quad \bar{w}_\square(\boldsymbol{u}^s) = 0, \quad \bar{\theta}_{\square,\alpha}(\boldsymbol{u}^s) = 0, \qquad (2.18)$$

$$\bar{h}_{\square,\alpha\beta}(\boldsymbol{u}^s) = 0, \quad \bar{g}_{\square,\alpha}(\boldsymbol{u}^s) = 0, \quad \bar{\kappa}_{\square,\alpha\beta}(\boldsymbol{u}^s) = 0 \qquad (2.19)$$

where $\mathbb{U}_\square^{\mathrm{s}}$ is a sufficiently smooth space, and where the homogenisation operators enters as constraints. These constraints can be enforced weakly with Lagrange parameters (i.e. Neumann), or strongly with Dirichlet or Periodic boundary conditions on $\Gamma_\square$. Note, however, that $\bar{\theta}_{\square,\alpha}(\boldsymbol{u})$ constitutes a volume constraint that can not be enforced with constraints on the boundary, and must therefore be enforced weakly using e.g. Lagrange parameters.

3 Macroscale: Robust modelling of delamination using adaptive isogeometric shell element

Delamination is a prominent failure mode in layered fibre composites, characterized by the propagation of cracks between layers. Experimental investigation has demonstrated that delamination occurs early in the failure process, subsequently influencing the mechanisms of failure, see e.g. Grauers et al. [29] on the crushing of laminated fibre composites. This finding underscores the necessity of incorporating delamination into models to achieve accurate simulations of fibre composite failure. However, modelling delamination presents significant computational challenges, as it often necessitates the use of high fidelity models. Consequently, there is a need for efficient tools to facilitate the modelling of delamination.

3.1 Adaptive modelling of layered composites

To address the challenges associated with efficiently modelling delamination in layered fibre composite structures, authors has devised adaptive models to limit the computational effort. The core idea behind adaptive simulation models, is to only use refined models (e.g. refined meshes) in areas where it is needed, while using a coarser modelling approach elsewhere. In the context of delamination, this means that a refined through-thickness discretisation (which can capture the separation of layers) is only used where the delamination event is active.

The use of adaptive finite element models for analysing delamination in layered fibre-reinforced composites is not a new concept, and various approaches have been proposed. For instance, in the work of Främby et al. [8], a quadratic triangular shell element with adaptive through-thickness refinement was developed for crash simulations in LS-DYNA. Moreover, in Trabal et al. [30], adaptive continuum elements with both in-plane and out-of-plane refinement capabilities were introduced through the floating node method to simulate delamination under high cycle fatigue. Both mentioned references demonstrated significant speed-up, when compared to fully resolved counterparts (i.e. models where each layer and cohesive zones are present from the beginning of the simulation).

3.2 Adaptive isogeometric shell element

In this thesis (and **Paper B**), an adaptive shell model is developed in an isogeometric (IGA) framework, which comes with some interesting advantages (outlined in Section 3.2.1). The main concepts of the present shell element can be summarised as follows:

- A shell formulation with spline basis functions from IGA is used to describe the midsurface geometry and undeformed configuration.

- A isogeometric continuum-shell formulation for describing the displacement field. An isogeometric framework allows for flexible control of the out-of-plane displacement discretisation, using the knot-insertion technique from IGA.

- The utilisation of the stress recovery method with the goal to improve the prediction of transverse stresses in elements with coarse through-thickness discretisation.

- Criteria based on the stress and damage state, to determine when the adaptive model requires refinement. These criteria are designed to trigger refinement only when necessary, thus enhancing computational efficiency while ensuring accuracy in regions subjected to high stress or progressed damage.

These points will be discussed in greater detail in the following subsections. However, before that, a discussion on isogeometric analysis and its relevance to shell modelling will be presented.

3.2.1 Notes on IGA and shell modelling

Isogeometric Analysis was first proposed in 2005 by Hughes et al. [31], with the aim of bridging the gap between Computer-Aided Design (CAD) and Computer-Aided Engineering (CAE). At the time, the process of translating CAD geometries into analysis-suitable meshes was considered to be one of the most time-consuming tasks for finite element analysts. Bridging the gap between CAD and CAE therefore offers significant potential to save both time and money. To facilitate this connection, it was proposed to utilise the basis functions used in the geometric description of CAD models (specifically spline functions such as B-splines or NURBS), directly as basis functions in the finite element approximation. Furthermore, another attractive benefit of this approach, is that no geometrical approximation would be introduced, as the splines can describe conical section such as holes exactly. The ultimate goal of having a seamless transition between CAD and CAE is however still an open question, mainly due to the CAD geometries often being non-suitable for analysis, which in turn requires pre-processing of the CAD geometry [32].

Regardless of the progress in closing the gap between CAD and CAE, the utilisation of spline functions for the FE approximation has shown to bring other benefits. Splines are by construction C^{p-1} continuous (where p is the order of the splines). In fact, B-splines provide higher order functions for the minimum number of DOFs, which makes higher order approximation especially efficient (via k-refinement [31]). Moreover, splines create a very smooth basis for the analysis, which has shown to provide beneficial properties in e.g. structural vibration problems [33]. Finally, the higher order continuity makes gradients (e.g. strains) continuous in the entire patch.

IGA has also been shown to bring advantages in shell modelling. Firstly, due to the at least C^1 continuity of the spline basis, it is straight-forward to implement classical Kirchhoff-Love theory. This has created a renaissance of Kirchhoff-Love formulations [34, 35], which has previously not been possible with C^0 Lagrange elements. In regard to Reissner-Mindlin type shells, Benson et al. [36] developed an IGA-based Reissner-Mindlin shell for linear elastic and non-linear dynamic analysis. Interestingly, the element is rather insensitive to shear locking (with mesh-refinement) without the need for special element-technologies for removing locking.
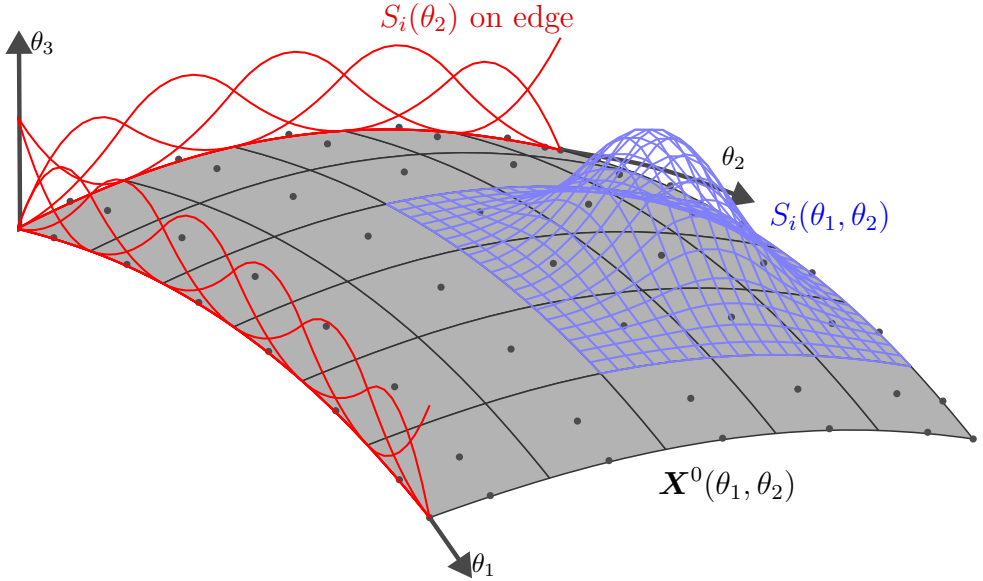
Figure 3.1: *A midsurface $\boldsymbol{X}^0$ described with B-Splines with 6×5 elements. Red curves represent the univariate splines in each parametric directions, and the blue function represents one of the B-splines functions ($S_2 5$) for the IGA mesh. Black dots are the control points.*

A considerable amount of research has also been devoted to IGA-based solid-shell elements, where the work presented in **Paper B** is positioned. In a series of publications [37–39], an isogeometric solid-shell element was developed, which forms the foundation for the adaptive shell element in **Paper B**. It has been demonstrated that with the use of higher-order and smooth spline bases, the element is rather insensitivity to locking. In related works by Caseiro et al. [40, 41], it was shown that classical locking alleviation techniques, such as the Assumed Natural Strain (ANS) method, can further suppress issues like shear and membrane locking. This allows the use of relatively coarse meshes with second-order basis functions while maintaining accuracy.

3.2.2 Shell geometry and Adaptive shell kinematics

The (geometric) input for the shell model is the midsurface, which is constructed using Spline functions. A midsurface and some spline functions are illustrated in Figure 3.1. The midsurface (of the undeformed configuration) is denoted $\boldsymbol{X}^0(\theta_1, \theta_2)$, and is described by a curve-linear coordinate system with coordinates θ_1, θ_2:

$$\boldsymbol{X}^0(\theta_1, \theta_2) = \sum_{i=1}^{N_{\text{cp}}} S_i(\theta_1, \theta_2)\hat{\boldsymbol{p}}_i. \tag{3.1}$$

Here, $S_i(\theta_1, \theta_2)$ are isogeometric spline basis functions (e.g. B-Splines, NURBS, T-Splines),

N_{cp} is the number of control points, and $\hat{\boldsymbol{p}}_i$ are positions of the control points. Using the midsurface as a base, we use standard shell theory to define co-variant and contra-variant base vectors, deformation gradient, and other related shell kinematic variables. For detailed information about the shell formulation, we refer to Adams et al. [39].

The underlying discretisation of the displacement field, $\boldsymbol{u}(\theta_1, \theta_2, \theta_3)$, of the shell element is described with a continuum-shell representation:

$$\boldsymbol{u}(\theta_1, \theta_2, \theta_3) = \sum_{I=1}^{N_u} N_I(\theta_1, \theta_2, \theta_3)\boldsymbol{a}_I, \tag{3.2}$$

where N_{u} are the total number of shape functions for the displacement field (in the current configuration), and $\boldsymbol{a}_I$ are displacement degrees of freedom. $N_I(\theta_1, \theta_2, \theta_3)$ are constructed as a combination of bivariate in-plane spline functions and univariate out-of-plane B-spline functions:

$$\begin{aligned} N_I &= S_i(\theta_1, \theta_2)H_j(\theta_3), \\ i &= [1, \ldots, N_{\mathrm{cp}}], \\ j &= [1, \ldots, m_i], \end{aligned} \tag{3.3}$$

For the in-plane functions, an isoperimetric formulation is used, i.e. we use the same spline function $S_i(\theta_1, \theta_2)$ used to describe the midsurface in Equation (3.1). Then, for each in-plane shape function (or control point), i, we associate with it a set of out-of-plane B-Spline functions $H_j(\theta_3)$. These out-of-plane shape functions are the heart of the adaptive shell formulation, as it is these that we adaptively refine in order to control the kinematics through the thickness. The refinement of the shape functions $H_j(\theta_3)$ is performed using knot-insertion, which is a technique used in IGA for mesh refinement and controlling the continuity of the B-spline basis functions.

Based on the refinement level of $H_j(\theta_3)$, we introduce three different configurations, which are dubbed *lumped*, *layered* and *discontinuous*. In order to describe the three different configurations, consider the case of a laminated structure with three layers and a set of second order (out-of-plane) shape-functions H_j.

lumped A control point in the *lumped* configuration, homogenises (lumps) all the layers in to one "element" through the thickness. This is similar to an ESL representation, which is known to predict in-plane stresses accurately and is relatively computational efficient. However, due to the coarse out-of-plane resolution (in this case only three control points through the thickness), a in-plane control point in the lumped configuration can not predict the transverse stresses normal to the midsurface with sufficient accuracy.
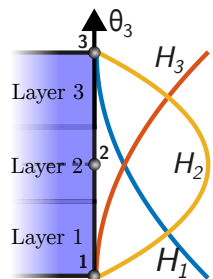
layered Using knot-insertion, the number of shape-function and their continuity can be controlled to obtain the *layered* configuration. Here, we desire C^0 continuity at the ply-interfaces to model the strain discontinuity between the layers, effectively becoming a LW model. The *layered* configuration increases the through-thickness accuracy (of e.g. stresses) significantly, however, as a consequence, becomes much more computationally demanding.
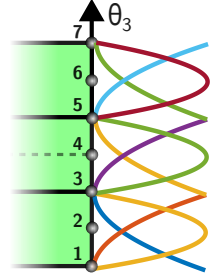
discontinuous The goal of the *discontinuous* control point configuration is to represent separation between the layers, in order to model delamination. The configuration is obtained by once again applying knot-insertion at layer coordinates where we want to insert C^{-1} continuity. Furthermore, cohesive zone elements are inserted in this configuration to capture the energy release rate during the delamination propagation.
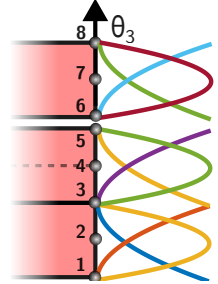
The three configurations presented above (*lumped*, *layered* and *discontinuous*) can now be used to adaptively refine the model. The shell model is initiated with control points in a *lumped* configuration, and then progressively refined as damage is detected and propagated. In this manner, a combination of an ELS and LW modelling approach is achieved, which will reduce the total computational effort of the model.

3.2.3 Refinement criteria

An important aspect of any adaptive method is to decide when a kinematical refinement of the model should be performed. In this thesis, we follow the work by Främby [42], in which two refinement criteria are proposed. The first criterion is based on the stress state, and is used to determine when a new delamination zone should be initiated. The criterion monitors the transverse stresses at the location of the interface between two adjacent plies:

$$\frac{\langle\sigma_{33}\rangle_+^2}{\sigma_{\mathrm{fn}}^2} + \frac{\sigma_{13}^2 + \sigma_{23}^2}{\sigma_{\mathrm{fs}}^2} \geq r_{\mathrm{I}}^2 \tag{3.4}$$

where σ_{fn} and σ_{fs} are the interlaminar normal and shear strengths, respectively, and Macaulay brackets $\langle\bullet\rangle_+$ are used as compressive stresses should not contribute to crack initiation. Moreover, r_{I} is a user-defined parameter between 0 and 1 which indicates when the configuration should be updated. Note that it is crucial to enhance the element (whether from *lumped* or *layered* to *discontinuous*) well before the quadratic failure criterion exceeds 1, ensuring that the newly introduced cohesive zone element does not immediately enter the damage zone upon insertion.

The second refinement criterion is used to determine when a delamination zone should propagate. In cohesive zone modelling, it is well established that the traction profile ahead of the crack tip significantly influences the behaviour of the cohesive zone [43]. Therefore, maintaining a number of elements in front of the cohesive zone in a *discontinuous* configuration is essential. At each converged time-step, the damage variables in the cohesive elements surrounding the crack front are monitored. If the damage state exceeds a predefined threshold (set by the user), a search is conducted in the vicinity of the element. Within the search radius, any *lumped* or *layered* elements are upgraded to a *discontinuous* state.

3.2.4   Stress recovery

As previously discussed, the coarse out-of-plane discretisation in the *lumped* elements results in poor predictions of the out-of-plane transverse stresses. This makes the *lumped* configuration inadequate to be used to predict when and at which ply-interface refinement is needed, according to the criterion in Equation (3.4). In order to improve the transverse stress prediction, a method known as stress recovery is used [44, 45]. The main idea of the stress recovery method is to re-compute the transverse stresses from the equilibrium equations and the in-plane stresses.

The stress recovery technique is now a well-established approach for enhancing stress predictions in ESL models. Numerous studies have demonstrated its effectiveness in the context of flat plates and shells [24, 46–48]. The usefulness of stress recovery in flat plates is however limited, as the transverse stresses in flat plates and shells are in many cases small compared to the in-plane stresses (see the results in e.g. [39]). However, in curved geometries, with the influence of curvature, the transverse stresses become more pronounced [49]. Due to the influence of curvature have on transverse stresses, authors have recently developed methods for stress recovery for curved shell. In Daniel et al [50], a stress recovery method was developed in curve-linear coordinates of the linear momentum balance equations. A closed form expression for the transverse stresses was obtained by considering the formulation in the principal curvature directions. With the same goal, Patton et al. [51] developed a stress recovery method for curved shells, but instead considered point-wise local Cartesian coordinate systems for the derivation of the framework.

For the current shell element, we use the stress recovery formulation for curved geometries, derived in Daniel et al.. Since our shell element is formulated in an isogeometric framework, we expect some advantages compared to standard finite elements. First, the higher continuity of the spline functions in IGA results in in-plane continuity of the stress field. This means that it is possible to obtain first and second order stress gradients directly in each material point (which is required for the stress recovery method). This is in contrast to standard finite elements where the C^0 basis requires patch-wise *least square* fitting to obtain accurate estimations of the stress gradients.
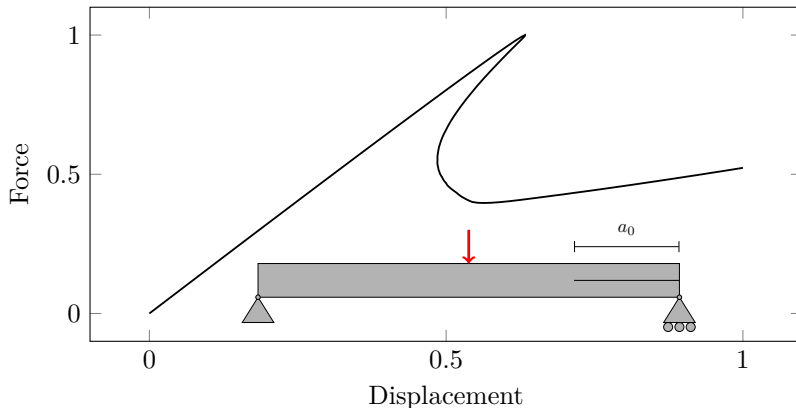
Figure 3.2: *Illustration of snap-back in a quasi-static simulation of an end-notch-flexure test.*

3.3 Dissipation based path-following solver

The initiation and propagation of delamination in layered composites is characterised by the release of significant amounts of stored elastic energy in the form of brittle and fast moving cracks. When simulating delamination using standard incremental Newton solvers in a quasi-static setting, convergence difficulties are frequently encountered. To exemplify this, consider the force-displacement curve from the end-notch flexure (ENF) test depicted in Figure 3.2. In this scenario, elastic energy accumulates as the applied force increases, until the limit of structure is reached, at which delamination begins to propagate. This leads to the structure exhibiting a "snap-back" response after the peak force is surpassed. This snap-back behaviour cannot be traced with a displacement or force controlled Newton solver, leading to the loss of valuable information regarding the post-peak response of the material.

To accurately trace the complete equilibrium path in problems with by brittle failure mechanisms within quasi-static simulations, it is necessary to employ so-called path-following solvers. These solvers, often referred to as arc-length solvers, have been extensively used within the computational mechanics community for analysing geometrically non-linear problems, such as buckling. Pioneering works on arc-length solvers were made by Wempner [52] and Riks [53]. Another class of path-following solvers, which have also gained widespread use, are dissipation-based path-following solvers. These solvers have been shown to efficiently handle problems involving material non-linearities, such as delamination and phase-field models [10, 54].

In **Paper C**, we develop an arc-length solver that is based on the local dissipation rate at each material point. This solver generalises the concept of dissipation-based arc-length methods, enabling the use of any material or damage model that can be formulated with a dissipation rate. We demonstrate that the solver efficiently addresses a wide range of problems involving non-linear material damage and failure. It is particularly effective for tracing the delamination of multiple layers in fibre composite structures.

3.3.1 Path-following solvers

In this section, we provide an overview of the basic equations used in path-following solvers. Consider the discretised governing equations in finite element form:

$$\boldsymbol{r}(\boldsymbol{a}) = \boldsymbol{f}^{\mathrm{int}}(\boldsymbol{a}) - \lambda\hat{\boldsymbol{f}}, \tag{3.5}$$

where $\boldsymbol{a}$ is a vector of unknown degrees of freedom (typically displacements), $\boldsymbol{r}(\boldsymbol{a})$ is the residual vector, $\boldsymbol{f}^{\mathrm{int}}$ is the internal force vector, λ is a load multiplier, and $\hat{\boldsymbol{f}}$ is a unit vector defining the direction of the forces. In a quasi-static simulations, Equation (3.5) is usually solved with Newton-Raphson iterations in a incremental manner, where the load parameter λ is controlled directly. In contrast, path-following solvers treat the load parameter as an additional unknown, reformulating the residual as a function of both $\boldsymbol{a}$ and λ, i.e., $\boldsymbol{r}(\boldsymbol{a}, \lambda)$. By solving for both variables simultaneously, path-following methods can trace the equilibrium path across the complete force-displacement space.

With the introduction of an additional unknown variable to the system, it becomes necessary to include an additional equation. This equation is known as the path-following constraint, $\varphi(\boldsymbol{a}, \lambda)$, and is generally expressed in the following form:

$$\varphi(\boldsymbol{a}, \lambda) = 0 \tag{3.6}$$

The constraint equation φ should depend on $\boldsymbol{a}$ (and potentially on λ as well) and must exhibit a monotonically increasing behaviour.

By combining Equation (3.5) and Equation (3.6), we arrive at the following system of equations:

$$\begin{bmatrix} \boldsymbol{r}(\boldsymbol{a}, \lambda) \\ \varphi(\boldsymbol{a}, \lambda) \end{bmatrix} = \begin{bmatrix} \boldsymbol{0} \\ 0 \end{bmatrix}. \tag{3.7}$$

By linearising the above equations, both λ and $\boldsymbol{a}$ can be incrementally solved using a Newton-Raphson scheme. This yields the following system of linearized equations:

$$\begin{bmatrix} \mathrm{d}\boldsymbol{a} \\ \mathrm{d}\lambda \end{bmatrix} = \begin{bmatrix} \boldsymbol{K} & -\hat{\boldsymbol{f}} \\ \boldsymbol{h}^T & w \end{bmatrix}^{-1} \begin{bmatrix} -\boldsymbol{r} \\ -\varphi \end{bmatrix}, \tag{3.8}$$

where $\mathrm{d}\boldsymbol{a}$ and $\mathrm{d}\lambda$ are the incremental updates in a Newton-Rapson scheme. Furthermore, the Jacobian consists of the following components:

$$\boldsymbol{K} = \frac{\partial \boldsymbol{f}^{\mathrm{int}}}{\partial \boldsymbol{a}}, \qquad \boldsymbol{h} = \frac{\partial \varphi}{\partial \boldsymbol{a}}, \qquad w = \frac{\partial \varphi}{\partial \lambda}. \tag{3.9}$$

Here, $\boldsymbol{K}$ is the standard tangent stiffness matrix, while $\boldsymbol{h}$ and w are additional terms that arise from the addition of the path-following constraint.

3.3.2 Dissipation based path-following constraint

In **Paper C**, we propose to express the path following constraint $\varphi(\boldsymbol{a})$ based on the dissipation rate of the problem:

$$\varphi(\boldsymbol{a}) = \int_\Omega \Delta D \, \mathrm{d}\Omega - \Delta\tau = 0, \tag{3.10}$$

where ΔD is the incremental energy dissipation between two load steps, and $\Delta\tau$ is used-defined parameter defining the allowed dissipation rate (step length) between two steps. Moreover, Ω is domain of interest where dissipation is active, e.g. in the bulk material or in an interface zone. The path following constraint in Equation (3.10) is formulated in a generic form, and requires that an explicit expression for ΔD exists (or can be formulated) for the failure mechanism in question. In **Paper C**, we demonstrate how the method can be applied for problems with large strain plasticity, phase-field damage and delamination. Furthermore, Equation (3.10) allows for several mechanisms to be considered simultaneously. However, if one failure mechanism dissipates less energy than the others, it will control the allowable size of the step-length $\Delta\tau$.

In terms of implementation, Equation (3.10) is computed for each element and quadrature point. This calculation can be performed either during the assembly of the element internal force vector or stiffness matrix, or in a separate assembly loop. Moreover, $\boldsymbol{h}$ is required. In the case of e.g. cohesive zone elements with the interface jump $\boldsymbol{J}$, the entries of $\boldsymbol{h}$ can be computed as:

$$h_I = \int_\Omega \frac{\partial \Delta D}{\partial \boldsymbol{J}} \cdot \frac{\partial \boldsymbol{J}}{\partial a_I} \, \mathrm{d}\Omega \tag{3.11}$$

where a_I are the entries of $\boldsymbol{a}$. The term $\frac{\partial \Delta D}{\partial \boldsymbol{J}}$ is most conveniently computed during the evaluation of the material response (i.e. in the material routine), and $\frac{\partial \boldsymbol{J}}{\partial a_I}$ is a quantity evaluated during the construction of the element local stiffness matrix.

4 Mesoscale: Modelling of complex fibre geometries using Finite Cell Method

Mesoscale modelling is employed to model the behaviour of materials at an intermediate level between the microscopic structure and the macroscopic response. In the context of fibre-reinforced textile composite materials, the mesoscale involves a detailed representation of the fibre bundles, matrix, and their interfaces. This level of modelling is particularly advantageous for fibre composites, as mesoscale features significantly influence the overall mechanical performance. Common applications of mesoscale modelling of fibre composites include estimation of effective mechanical properties [12], or investigation into failure and damage [13].

In Lomov et al. [55], a road map with key steps for FE modelling of mesoscale textile composites is outlined.

1. Building a model of the internal geometry of the reinforcement

2. Transferring the geometry into a volume description

3. Preparation for meshing: correction of the interpenetration of volumes of yarns in the solid model and providing space for the thin matrix layers between the yarns

4. Meshing

5. Assigning local material properties to the impregnated yarns and the matrix;

6. Definition of the minimum possible unit cell using symmetry of the reinforcement and assigning periodic boundary conditions

7. Homogenisation procedure

8. Damage initiation criteria

9. Damage propagation modelling

From this road map, it is evident that a substantial amount of effort is invested in model creation (steps 1-4). Therefore, it is important to establish an efficient model creation process. In **Paper D**, we focus on a method for simplifying the meshing processes in step 4, which is particularly challenging for textile fibre composites. However, we first review common tools used to generate the mesoscale geometries (steps 1–3).

4.1 Generation of mesoscale structure

The first step in analysing the mesoscale structure of fibre composites, or any other material sub-structure for that matter, is the generation of the corresponding geometry. This task is far from straightforward, and multiple approaches for generating the mesoscale geometries for various textile fibre architectures has been proposed.

A common approach is to generate idealised geometries based on basic geometric shapes and curves. For instance, tools such as TexGen [15] and WiseTex [16] can be used to create geometries for woven composites, accommodating both two-dimensional and three-dimensional weaves, see Figure 4.1 for an example of a 3D-woven composite. The mesoscale geometries are relatively fast to generate, but may often contain intersections which needs to be resolved before being used in mechanical simulations.

Another method for generating the mesoscale structure of fibre composites involves process modelling [19]. A popular approach in this category is the digital chain method [17], where fibre bundles are represented by multiple chains of 1D beam elements (using a finite amount of beam-chains per bundle). Unlike the idealised geometry generation, process simulation introduces randomness and imperfections, and results in more realistic geometries. Process modelling is typically computationally intensive, and converting the digital-chain bundles into a solid representation suitable for simulations is non-trivial.

A third method involves generating mesoscale structures based on CT-scan data. This approach provides geometrically exact models, incorporating realistic voids and defects, as it is derived from real samples. For early work on this topic, see [56].

4.2 Discretisation of textile fibre composite structures at the mesoscale

Regardless of the method employed to generate the mesoscale structure, the resulting geometry is typically complex. Fibre bundles or reinforcements are often intertwined and form narrow regions, which makes the generation of meshes particularly challenging. This difficulty has been consistently reported in the literature [55, 57, 58]. The challenge of producing high-quality meshes is further evidenced by the widespread use of voxel meshes for discretising mesoscale structures by many authors, see e.g. [59, 60]. The generation of voxel meshes can be automatised, but do have inherent flaws [20].

There is a clear need for improved discretisation process for complex mesoscale structures. In response to this, researchers have explored enhancements to traditional meshing techniques to produce boundary-conforming tetrahedral meshes, see Li et al [61] or Zhang et al. [62]. Alternatively, a popular method that is often touted for its ability to simplify the meshing procedure, is Immersed Boundary Methods. Many versions of immersed boundary methods has been developed, e.g. Finite Cell Method [63] (FCM) and CutFEM [64] to name a few. The core concept behind these methods is to simplify meshing by immersing, or embedding, the geometry into a simple, rectilinear background grid. This makes the process of creating a discretisation automatic, which is highly beneficial when a standard meshing procedure would be to time intensive or cumbersome. A drawback with Immersed boundary methods, however, is that the background grid does not conform to the boundaries of the geometry, resulting in some of elements being cut or trimmed by the geometry. Consequently, special numerical integration rules are required to handle the integration of these cut elements.

In **Paper D**, we investigate the use of FCM for modelling of fibre composite mesoscale structures. The important steps of the method is outlined in the following sections.

Figure 4.1: *SVE of a 3D fibre composite generated by Texgen.*

## 4.3 Discretisation of textile fibre composite mesoscale structures using Finite Cell Method

With the geometric description of the mesoscale structure in-place (following section 4.1 and possibly steps 1-3 in the road map), the next step is to create a discretisation. First, we propose meshing the fibre bundle (or reinforcements) independently, using boundary-fitted elements (e.g. tetrahedral or hexahedral elements). It is important to note that fibre bundles are often relatively simple geometrical structures, typically composed of cylindrical tubes, which does not pose large problems for meshing tools. As an illustration, we use here a unit-cell of a woven composite, see Figure 4.2a. Here, the geometry of the woven composite is represented with B-Splines, and can therefore be utilised directly as the boundary-fitted mesh (after appropriate mesh refinement with knot-insertion).

Next, we embed/immerse the bundle geometry in a FCM background grid, see Figure 4.2b. The background grid will act as the basis for the discretisation of the matrix. The background mesh can consist of e.g. standard hexahedral Lagrange elements, however, here we opt for the use of IGA elements with higher order continuity spline functions. Many of the elements in the FCM background grid will be fully contained in the reinforcement phase. These elements and their corresponding shape functions, will not contribute to the displacement field of the matrix, and may therefore be discarded. The final version of the FCM mesh for the matrix phase is seen in Figure 4.2c.

At this point, we have a set of uncoupled meshes; the individual (boundary-fitted) meshes for the bundles, and the unfitted background grid for the matrix. These individual meshes need to be coupled in some way. Firstly, for the interfaces between the bundles and the matrix, we assume that they are perfectly bonded, and model that with the use of a penalty-based interface constraint. Next, the bundle-bundle interfaces are assumed to be coupled through a cohesive interface. Note, however, that we here only consider linear elasticity, which means that the linear cohesive interface is the same as a standard penalty constraint. In future application this may be extended to non-linear cohesive zone laws. Furthermore, note that the discretization of the bundles are independent, which means that the interface meshes are non-matching. This means that the cohesive zone interface needs to be applied with a mortar-type approach, where the interface constraint is integrated on one of the bundle sides.
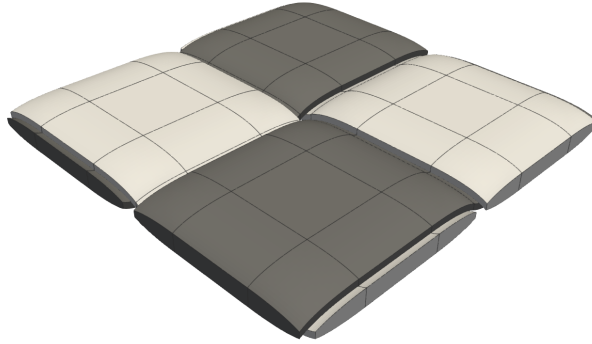
(a) *Bundles (2d woven textile composite).*
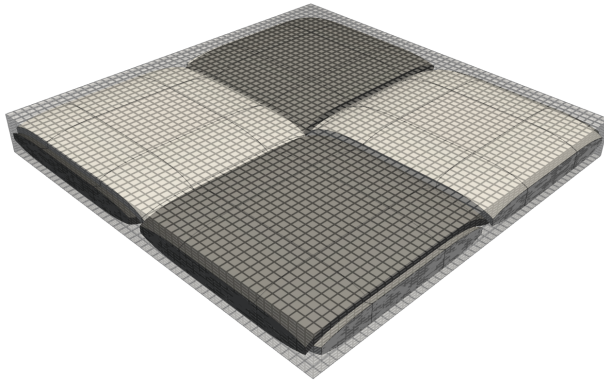
(b) *Immersed bundles in FCM background grid.*
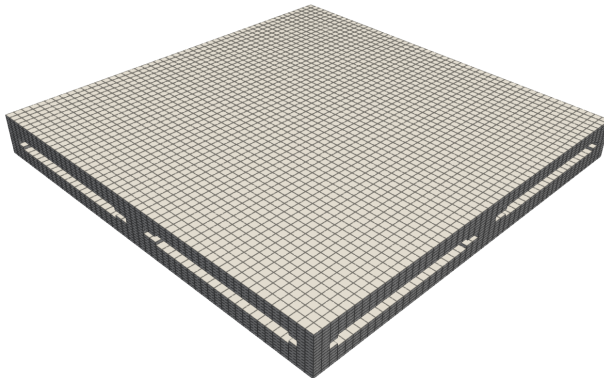
(c) *Resulting unfitted background grid for the matrix.*

Figure 4.2: *The automatised process of creating a discretisation for the matrix phase.*

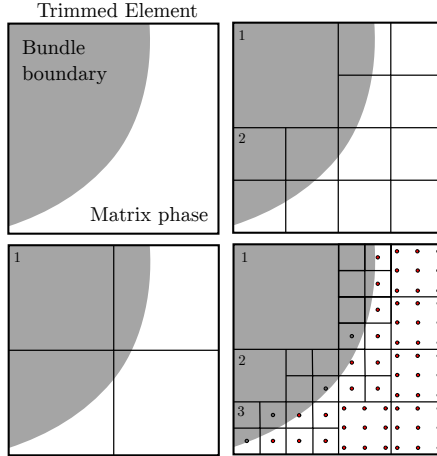Figure 4.3: *Process for creating new numerical integration schemes for trimmed elements. The collection of all quadrature points in the sub-cells are used for volume integration of the trimmed elements.*

4.3.1 Numerical treatment of non boundary-fitted discretisation

An unavoidable consequence of the matrix discretisation being non-boundary-fitted is that some elements will be intersected by the boundaries of the fibre bundles. These intersected elements, often referred to as trimmed elements, cannot be treated using standard numerical integration rules for operations such as volume integrals. Instead, specialised integration rules must be developed for these elements. One approach to generating such specialised quadrature rules involves subdividing the trimmed element into smaller sub-cells, where the sub-cells are subsequently used to build quadrature rules within each sub-cell, see Figure 4.3. This subdivision is often performed recursively, using methods such as quad-trees in 2D and octrees in 3D [65].

Another unavoidable consequence of using unfitted boundary meshes is that some trimmed elements may become arbitrarily small, particularly in cases of arbitrary mesh refinement. This phenomenon is known to result in ill-conditioned systems and stability issues. Consequently, significant research has been devoted to developing stability methods [66]. One widely adopted approach to stabilise the solutions, is the α-stabilisation method [67], where artificial stiffness is introduced to the problematic elements. Another approach, employed in **Paper D**, is the ghost penalty method [68]. This method penalises jumps in displacement gradients across element faces of the affected trimmed elements. By doing so, it suppresses large jumps in displacement gradients, which are common in ill-conditioned trimmed elements. A feature of the ghost penalty method is that it mitigates issues related to ill-conditioned matrices and stability, while also maintaining variational consistency.

5 Concluding remarks and outlook

The present work is concerned with numerical methods for multiscale modelling of fibre composites. The thesis is divided into three main parts; computational homogenisation, macroscale modelling, and mesoscale modelling.

In order to couple the macroscale and mesoscale, it is essential to use kinematically consistent prolongation and homogenisation conditions. These coupling conditions are however not always trivial to postulate, for example when considering shell and plate kinematics. Therefore, it is important with mathematical frameworks that facilitate a consistent derivation procedure. To this extent, we demonstrate in **Paper A** that VCH can be used to derive a kinematically consistent homogenisation framework for plates, and that appropriate coupling conditions are obtained. Specifically, we derive appropriate homogenisation condition for the transverse shear angles (or cross-sectional rotations), which lead to size independent results with respect to the homogenised shear stiffness.

The plate-based homgenisation framework is currently limited to small strains and flat structures. As an outlook,

In **Paper B**, we develop an adaptive isogeometric shell element for the modelling of delamination. Based on our findings, several conclusions can be drawn. First, we observe that the stress recovery method performs well within the isogeometric framework. The C^1 continuous stresses allow for straightforward computation of stress gradients on a element-local level, a feature not present with C^0 Lagrange elements. Additionally, geometrical properties such as curvature, which are essential for the stress recovery method, are represented exactly in isogeometric analysis (IGA), further enhancing accuracy. With respect to the adaptive aspects associated with the isogeometric shell element, we conclude that the overhead coming from the (i) stress recovery method and (ii) checking the refinement criteria, is justifiable. Based on the numerical results of the paper, we demonstrate that a speed-up factor of 1.3 is obtained (when compared to a fully resolved model), in a problem with a four layered cantilever beam with two propagation cracks. Additional speed gains are expected when the number of layers in the composite structure increases, or when the size of the delamination zone is small compared to the rest of the structure.

The adaptive shell element capabilities are currently only demonstrated on rather small problems. As an outlook, we would like to apply the shell element to larger and more industrial applications. Here, interesting aspects relating to numerical implementation will become relevant, such as how to efficiently represent adaptive data structures, efficient solution of the linear systems, and more. Furthermore, when applying the adaptive shell element to more realistic problems, the significance of other failure mechanisms than delamination will increase. Indeed, intralaminar damage (such as tansverse matrix cracking) are often a pre-cursor to delamination, and this interplay is important to capture. Intralaminar damage can be modelled with both discrete and smeared crack models. In the current setting, smeared crack models is most straightforward to implement, as the adaptive element can incorporate any constitutive models within the individual layers. It does not, however, have the kinematic capabilities to represent discrete through-thickness cracks.

To address the challenges of brittle material damage and fracture in quasi-static

simulations, in **Paper C**, we introduce an arc-length solver that leverages the material dissipation rate. This solver allows for robust tracing of the equilibrium path in a range of damage and material models, including cohesive zone damage, phase-field damage, and large-strain plasticity. At the moment, the solver is limited to rate-independent problems, which restricts its applicability scenarios involving cyclic loading or rate-dependent material models. As an outlook, we would therefore like to extend the solver to also include time evolution. This extension poses an interesting challenge, as the concept of time in quasi-static simulations is somewhat artificial. A potential approach to address this, is to make the (pseudo) time variable dependent on the dissipation rate, thereby enuring that the time variable is monotonically increasing.

In **Paper D**, we investigate the application of immersed methods for modelling fibre-reinforced mesoscale structures. Based on the numerical examples, we conclude that the proposed modelling approach offers a viable alternative for linear elastic simulations, such as analysing stresses and strains or predicting elastic stiffness. Compared to voxel-based methods, the immersed approach predicts the stress distribution more accurately, avoiding the erroneous stress peaks that often arise from the step-like nature of voxel discretisation. However, a significant drawback of the proposed method is the large number of quadrature points generated for the unfitted matrix discretisation, which increases computational demand. While this challenge is manageable for linear and static simulations, it will lead to substantial computational costs, both in memory and processing time, when applied to non-linear simulations. Further research is therefore necessary to optimise the framework for efficient non-linear analysis. In this context, the development of more efficient adaptive integration schemes, such as moment fitting, could be highly beneficial.

The homogenisation framework for plates in **Paper A**, the adaptive shell element at the macroscale in **Paper B**, and the mesoscale modelling framework in **Paper D** can be viewed as independent methods that has not been demonstrated to work in unisent. As an outlook, it we would like to combine these methods in a coupled two-scale modelling framework. Here, the multiscale vision can be adopted, wherein the macroscopic structure would be modelled using adaptive isogeometric shell elements, while damage initiation and propagation (whether interlaminar or intralaminar) would be informed by detailed mesoscale modelling. The plate-based homogenisation framework would serve as the link between the two scales. Homogenisation of damage does, however, presents notable challenges, as the fundamental assumptions of *separation of scale* breaks down. In this regard, the work of Svenning et al. [69] on the multiscale modelling of ductile fracture provides valuable guidance for addressing these issues.

References

[1] W. Zhang and J. Xu. Advanced lightweight materials for Automobiles: A review. *Materials and Design* **221** (2022), 110994. DOI: 10.1016/j.matdes.2022.110994.

[2] *Aero QTR_04, Boeing 787 from the ground up.* http://www.lb.boeing.com/commercial/aeromagazine/articles/qtr_4_06/article_04_2.html. 2006.

[3] S. Pinho et al. Material and structural response of polymer-matrix fibre-reinforced composites. *Journal of Composite Materials* **46**.19-20 (2012), 2313–2341. DOI: 10.1177/0021998312454478.

[4] M. Geers, V. Kouznetsova, and W. Brekelmans. Multi-scale computational homogenization: Trends and challenges. *Journal of Computational and Applied Mathematics* **234**.7 (2010), 2175–2182. DOI: 10.1016/j.cam.2009.08.077.

[5] S. Klarmann, F. Gruttmann, and S. Klinkel. Homogenization assumptions for coupled multiscale analysis of structural elements: beam kinematics. *Computational Mechanics* **65** (2020), 635–661. DOI: 10.1007/s00466-019-01787-z.

[6] M. Müller, S. Klarmann, and F. Gruttmann. A new homogenization scheme for beam and plate structures without a priori requirements on boundary conditions. *Computational Mechanics* **70**.6 (2022), 1167–1187. DOI: 10.1007/s00466-022-02219-1.

[7] E. W. C. Coenen, V. G. Kouznetsova, and M. G. D. Geers. Computational homogenization for heterogeneous thin sheets. *International Journal for Numerical Methods in Engineering* **83**.8-9 (2010), 1180–1205. DOI: 10.1002/nme.2833.

[8] J. Främby, M. Fagerström, and J. Brouzoulis. Adaptive modelling of delamination initiation and propagation using an equivalent single-layer shell approach. *International Journal for Numerical Methods in Engineering* **112**.8 (2017), 882–908. DOI: 10.1002/nme.5536.

[9] A. Soto et al. Low velocity impact and compression after impact simulation of thin ply laminates. *Composites Part A: Applied Science and Manufacturing* **109** (2018), 413–427. DOI: 10.1016/j.compositesa.2018.03.017.

[10] C. V. Verhoosel, J. J. C. Remmers, and M. A. Gutiérrez. A dissipation-based arc-length method for robust simulation of brittle and ductile failure. *International Journal for Numerical Methods in Engineering* **77**.9 (2009), 1290–1321. DOI: 10.1002/nme.2447.

[11] L. Gulfo et al. A 3D voxel-based mesostructure generator for finite element modelling of tow-based discontinuous composites. *Composites Part B: Engineering* **278** (2024), 111405. DOI: 10.1016/j.compositesb.2024.111405.

[12] C. Oddy et al. Predicting damage initiation in 3D fibre-reinforced composites – The case for strain-based criteria. *Composite Structures* **230** (2019), 111336. DOI: 10.1016/j.compstruct.2019.111336.

[13] H. K. Adluru et al. Performance prediction of interlock woven composites by independent mesh method. *Composites Part A: Applied Science and Manufacturing* **165** (2023), 107317. DOI: 10.1016/j.compositesa.2022.107317.

[14] S. V. Lomov et al. Full-field strain measurements for validation of meso-FE analysis of textile composites. *Composites Part A: Applied Science and Manufacturing* **39**.8

(2008). Full-field Measurements in Composites Testing and Analysis, 1218–1231. DOI: 10.1016/j.compositesa.2007.09.011.

[15] A. Long and L. Brown. "8 - Modelling the geometry of textile reinforcements for composites: TexGen". *Composite Reinforcements for Optimum Performance*. Ed. by P. Boisse. Woodhead Publishing Series in Composites Science and Engineering. Woodhead Publishing, 2011, pp. 239–264. DOI: 10.1533/9780857093714.2.239.

[16] I. Verpoest and S. V. Lomov. Virtual textile composites software WiseTex: Integration with micro-mechanical, permeability and structural analysis. *Composites Science and Technology* **65**.15 (2005). 20th Anniversary Special Issue, 2563–2574. DOI: 10.1016/j.compscitech.2005.05.031.

[17] G. Zhou, X. Sun, and Y. Wang. Multi-chain digital element analysis in textile mechanics. *Composites Science and Technology* **64** (2 2004), 239–244. DOI: 10.1016/S0266-3538(03)00258-6.

[18] S. Green et al. Numerical modelling of 3D woven preform deformations. *Composite Structures* **108** (2014), 747–756. DOI: 10.1016/j.compstruct.2013.10.015.

[19] J. P.-H. Belnoue and S. R. Hallett. Process models: A cornerstone to composites 4.0. *Composites Part B: Engineering* **283** (2024), 111621. DOI: 10.1016/j.compositesb.2024.111621.

[20] A. Doitrand et al. Comparison between voxel and consistent meso-scale models of woven composites. *Composites Part A: Applied Science and Manufacturing* **73** (2015), 143–154. DOI: 10.1016/j.compositesa.2015.02.022.

[21] F. Stig and S. Hallström. A modelling framework for composites containing 3D reinforcement. *Composite Structures* **94**.9 (2012), 2895–2901. DOI: https://doi.org/10.1016/j.compstruct.2012.03.009.

[22] M. G. Geers, E. W. Coenen, and V. G. Kouznetsova. Multi-scale computational homogenization of structured thin sheets. *Modelling and Simulation in Materials Science and Engineering* **15**.4 (2007), S393. DOI: 10.1088/0965-0393/15/4/S06.

[23] R. Larsson and M. Landervik. A stress-resultant shell theory based on multiscale homogenization. *Computer Methods in Applied Mechanics and Engineering* **263** (2013), 1–11. DOI: 10.1016/J.CMA.2013.04.011.

[24] J. Främby, J. Brouzoulis, and M. Fagerström. Assessment of two methods for the accurate prediction of transverse stress distributions in laminates. *Composite Structures* **140** (2016), 602–611. DOI: 10.1016/j.compstruct.2015.12.036.

[25] A. K. Hii and B. El Said. A kinematically consistent second-order computational homogenisation framework for thick shell models. *Computer Methods in Applied Mechanics and Engineering* **398** (2022), 115136. DOI: 10.1016/j.cma.2022.115136.

[26] F. Larsson, K. Runesson, and F. Su. Variationally consistent computational homogenization of transient heat flow. *International Journal for Numerical Methods in Engineering* **81**.13 (2009), 1659–1686. DOI: 10.1002/nme.2747.

[27] V. Tu et al. Variationally consistent homogenization of electrochemical ion transport in a porous structural battery electrolyte. *European Journal of Mechanics - A/Solids* **98** (2023), 104901. DOI: 10.1016/j.euromechsol.2022.104901.

[28] A. Sciegaj et al. A multiscale model for reinforced concrete with macro-scopic variation of reinforcement slip. *Computational Mechanics* **63**.8-9 (2019), 1432–0924. DOI: 10.1007/s00466-018-1588-3.

[29] L. Grauers, R. Olsson, and R. Gutkin. Energy absorption and damage mechanisms in progressive crushing of corrugated NCF laminates: Fractographic analysis. *Composite Structures* **110** (2014), 110–117. DOI: `10.1016/j.compstruct.2013.11.001`.

[30] G. G. Trabal et al. An adaptive floating node based formulation for the analysis of multiple delaminations under high cycle fatigue loading. *Composites Part A: Applied Science and Manufacturing* **160** (2022), 107036. DOI: `10.1016/j.compositesa.2022.107036`.

[31] T. Hughes, J. Cottrell, and Y. Bazilevs. Isogeometric analysis: CAD, finite elements, NURBS, exact geometry and mesh refinement. *Computer Methods in Applied Mechanics and Engineering* **194**.39 (2005), 4135–4195. DOI: `10.1016/j.cma.2004.10.008`.

[32] B. Marussig and T. J. R. Hughes. A Review of Trimming in Isogeometric Analysis: Challenges, Data Exchange and Simulation Aspects. *Archives of Computational Methods in Engineering* **25**.4 (2017), 1059–1127. DOI: `10.1007/s11831-017-9220-9`.

[33] J. Cottrell et al. Isogeometric analysis of structural vibrations. *Computer Methods in Applied Mechanics and Engineering* **195**.41 (2006), 5257–5296. DOI: `10.1016/j.cma.2005.09.027`.

[34] J. Kiendl et al. Isogeometric shell analysis with Kirchhoff–Love elements. *Computer Methods in Applied Mechanics and Engineering* **198**.49 (2009), 3902–3914. DOI: `10.1016/j.cma.2009.08.013`.

[35] D. Benson et al. A large deformation, rotation-free, isogeometric shell. *Computer Methods in Applied Mechanics and Engineering* **200**.13 (2011), 1367–1378. DOI: `10.1016/j.cma.2010.12.003`.

[36] D. Benson et al. Isogeometric shell analysis: The Reissner–Mindlin shell. *Computer Methods in Applied Mechanics and Engineering* **199**.5 (2010). Computational Geometry and Analysis, 276–289. DOI: `10.1016/j.cma.2009.05.011`.

[37] S. Hosseini et al. An isogeometric solid-like shell element for nonlinear analysis. *International Journal for Numerical Methods in Engineering* **95**.3 (2013), 238–256. DOI: `10.1002/nme.4505`.

[38] S. Hosseini et al. An isogeometric continuum shell element for non-linear analysis. *Computer Methods in Applied Mechanics and Engineering* **271** (2014), 1–22. DOI: `10.1016/j.cma.2013.11.023`.

[39] C. Adams, M. Fagerström, and J. J. C. Remmers. Efficient modelling of delamination growth using adaptive isogeometric continuum shell elements. *Computational Mechanics* **65**.1 (2019), 99–117. DOI: `10.1007/s00466-019-01754-8`.

[40] J. Caseiro et al. Assumed Natural Strain NURBS-based solid-shell element for the analysis of large deformation elasto-plastic thin-shell structures. *Computer Methods in Applied Mechanics and Engineering* **284** (2015). Isogeometric Analysis Special Issue, 861–880. DOI: `10.1016/j.cma.2014.10.037`.

[41] J. F. Caseiro et al. On the Assumed Natural Strain method to alleviate locking in solid-shell NURBS-based finite elements. *Computational Mechanics* **53**.6 (2014), 1341–1353. DOI: `10.1007/s00466-014-0978-4`.

[42] J. Främby. "Methods for efficient modelling of progressive failure in laminated fibre-reinforced composites". Available at `https://research.chalmers.se/en/`

publication/514650. PhD thesis. Gothenburg: Chalmers University of Technology, 2020.

[43] A. Turon et al. An engineering solution for mesh size effects in the simulation of delamination using cohesive zone models. *Engineering Fracture Mechanics* **74**.10 (2007), 1665–1682. DOI: `10.1016/j.engfracmech.2006.08.025`.

[44] R. Rolfes, K. Rohwer, and M. Ballerstaedt. Efficient linear transverse normal stress analysis of layered composite plates. *Computers & Structures* **68**.6 (1998), 643–652. DOI: `10.1016/S0045-7949(98)00097-2`.

[45] R. Rolfes and K. Rohwer. Improved transverse shear stresses in composite finite elements based on first order shear deformation theory. *International Journal for Numerical Methods in Engineering* **40**.1 (1997), 51–60. DOI: `10.1002/(SICI)1097-0207(19970115)40:1<51::AID-NME49>3.0.CO;2-3`.

[46] A. Patton et al. Fast and accurate elastic analysis of laminated composite plates via isogeometric collocation and an equilibrium-based stress recovery approach. *Composite Structures* **225** (2019), 111026. DOI: `10.1016/j.compstruct.2019.111026`.

[47] J.-E. Dufour et al. A cost-effective isogeometric approach for composite plates based on a stress recovery procedure. *Composites Part B: Engineering* **138** (2018), 12–18. DOI: `10.1016/j.compositesb.2017.11.026`.

[48] A. Patton, S. Faroughi, and A. Reali. Efficient equilibrium-based stress recovery for isogeometric laminated Euler–Bernoulli curved beams. *Composite Structures* **345** (2024), 118374. DOI: `10.1016/j.compstruct.2024.118374`.

[49] J.-S. Charrier et al. Determination of the out-of-plane tensile strength using four-point bending tests on laminated L-angle specimens with different stacking sequences and total thicknesses. *Composites Part A: Applied Science and Manufacturing* **81** (2016), 243–253. DOI: `10.1016/j.compositesa.2015.11.018`.

[50] P. M. Daniel et al. Complete transverse stress recovery model for linear shell elements in arbitrarily curved laminates. *Composite Structures* **252** (2020), 112675. DOI: `10.1016/j.compstruct.2020.112675`.

[51] A. Patton et al. Efficient equilibrium-based stress recovery for isogeometric laminated curved structures. *Composite Structures* **272** (2021), 113975. DOI: `10.1016/J.COMPSTRUCT.2021.113975`.

[52] G. A. Wempner. Discrete approximations related to nonlinear theories of solids. *International Journal of Solids and Structures* **7**.11 (1971), 1581–1599. DOI: `10.1016/0020-7683(71)90038-2`.

[53] E. Riks. The Application of Newton's Method to the Problem of Elastic Stability. *Journal of Applied Mechanics* **39**.4 (1972), 1060–1065. DOI: `10.1115/1.3422829`.

[54] R. Bharali, F. Larsson, and R. Jänicke. A micromorphic phase-field model for brittle and quasi-brittle fracture. *Computational Mechanics* **73**.3 (2023), 579–598. DOI: `10.1007/s00466-023-02380-1`.

[55] S. V. Lomov et al. Meso-FE modelling of textile composites: Road map, data flow and algorithms. *Composites Science and Technology* **67**.9 (2007), 1870–1891. DOI: `10.1016/j.compscitech.2006.10.017`.

[56] Y. Sinchuk et al. X-ray CT based multi-layer unit cell modeling of carbon fiber-reinforced textile composites: Segmentation, meshing and elastic property homoge-

nization. *Composite Structures* **298** (2022), 116003. DOI: `10.1016/j.compstruct.2022.116003`.

[57] E. V. Iarve et al. Independent mesh method-based prediction of local and volume average fields in textile composites. *Composites Part A: Applied Science and Manufacturing* **40** (12 2009), 1880–1890. DOI: `10.1016/J.COMPOSITESA.2009.04.034`.

[58] S. Green et al. Mechanical modelling of 3D woven composites considering realistic unit cell geometry. *Composite Structures* **118** (2014), 284–293. DOI: `10.1016/j.compstruct.2014.07.005`.

[59] Y. Cao et al. Predicting the tensile and compressive failure behavior of angle-ply spread tow woven composites. *Composite Structures* **234** (2020), 111701. DOI: `10.1016/J.COMPSTRUCT.2019.111701`.

[60] S. Yan, X. Zeng, and A. Long. Meso-scale modelling of 3D woven composite T-joints with weave variations. *Composites Science and Technology* **171** (2019), 171–179. DOI: `10.1016/j.compscitech.2018.12.024`.

[61] A. Li et al. A level set-based procedure for the cohesive modeling of yarn–yarn contacts in woven composite RVEs. *Composite Structures* **304** (2023), 116356. DOI: `https://doi.org/10.1016/j.compstruct.2022.116356`.

[62] P. Zhang et al. An integrated microstructure reconstruction and meshing framework for finite element modeling of woven fiber-composites. *Computer Methods in Applied Mechanics and Engineering* **422** (2024), 116797. DOI: `https://doi.org/10.1016/j.cma.2024.116797`.

[63] D. Schillinger and M. Ruess. The Finite Cell Method: A Review in the Context of Higher-Order Structural Analysis of CAD and Image-Based Geometric Models. *Archives of Computational Methods in Engineering* **22** (3 2015), 391–455. DOI: `10.1007/S11831-014-9115-Y/FIGURES/87`.

[64] E. Burman et al. CutFEM: Discretizing geometry and partial differential equations. *International Journal for Numerical Methods in Engineering* **104** (7 2015), 472–501. DOI: `10.1002/NME.4823`.

[65] A. Abedian et al. Performance of Different Integration Schemes in facing Discontinuities in the Finite Cell Method. *International Journal of Computational Methods* **10**.03 (2013), 1350002. DOI: `10.1142/S0219876213500023`.

[66] F. de Prenter et al. Stability and Conditioning of Immersed Finite Element Methods: Analysis and Remedies. *Archives of Computational Methods in Engineering* **30** (6 2023), 3617–3656. DOI: `10.1007/S11831-023-09913-0/FIGURES/9`.

[67] J. Parvizian, A. Düster, and E. Rank. Finite cell method: h- and p-extension for embedded domain problems in solid mechanics. *Computational Mechanics* **41**.1 (2007), 121–133. DOI: `10.1007/s00466-007-0173-y`.

[68] E. Burman and P. Hansbo. Fictitious domain finite element methods using cut elements: II. A stabilized Nitsche method. *Applied Numerical Mathematics* **62**.4 (2012). Third Chilean Workshop on Numerical Analysis of Partial Differential Equations (WONAPDE 2010), 328–341. DOI: `10.1016/j.apnum.2011.01.008`.

[69] E. Svenning. "Methods for efficient modelling of progressive failure in laminated fibre-reinforced composites". Available at `https://research.chalmers.se/en/publication/249319`. PhD thesis. Gothenburg: Chalmers University of Technology, 2017.

[74] B. G. F. Wei Tan and M. Price. Predicting the crushing behaviour of composite material using high-fidelity finite element modelling. *International Journal of Crashworthiness* **20**.1 (2015), 60–77. DOI: 10.1080/13588265.2014.972122.